

Mutual Information Matrix for Interpretable Fault Detection

Feiya Lv^a, Shujian Yu^{b,1}, Chenglin Wen^c, Jose C. Principe^b

^a*School of Software Engineering, Anyang Normal University, Anyang 455000, PR China*

^b*Department of Electrical and Computer Engineering, University of Florida, Gainesville, FL 32611, USA*

^c*School of Automation, Hangzhou Dianzi University, Hangzhou 310018, PR China*

Abstract

This paper presents a novel mutual information (MI) matrix based method for fault detection. Given a m -dimensional fault process, the MI matrix is a $m \times m$ matrix in which the (i, j) -th entry measures the MI values between the i -th dimension and the j -th dimension variables. We demonstrate that the transformed components extracted from the obtained MI matrix can precisely unveil the dynamics of the underlying (possibly nonlinear) process, thus offering a reliable indicator to the occurrence of different types of faults. We also suggest that the recently proposed matrix-based Rényi's α -entropy is a good surrogate to the classical Shannon's entropy in MI estimation. Experiments on both synthetic data and the benchmark Tennessee Eastman process demonstrate the interpretability of our methodology in identifying the root variables that cause the faults, and the superiority of our methodology in terms the improved fault detection rate (FDR) and the lowest false alarm rate (FAR).

Keywords: fault detection, mutual information matrix, matrix-based Rényi's α -entropy, transformed component analysis, interpretability.

1. Introduction

With the growing demand for security equipments and high-quality products, process monitoring has received tremendous attention in both academia and industry in the past decades. Among numerous problems in process monitoring, the fault detection, i.e., the identification of the presence of abnormal operating conditions in real-time, becomes an active topic. As data-driven approach requires neither model assumption nor a-priori information on data, it has been the main stream for fault detection and tolerance control in recent years [1, 2]. The multivariate statistical process monitoring (MSPM) is a well-known data-driven approach, and has been widely used in complex industrial environments [3, 4, 5].

Email addresses: lvfeiya0215@126.com (Feiya Lv), yusj1cy9011@ufl.edu (Shujian Yu), wenc1@hdu.edu.cn (Chenglin Wen), principe@cnel.ufl.edu (Jose C. Principe)

¹Corresponding author.

Traditional MSPM methods, e.g., principle component analysis (PCA) [6], partial least squares (PLS) [7] and independent component analysis (ICA) [8], take advantage of the Hotelling T^2 statistic in principle component subspace or the squared prediction error (SPE) statistic in residual subspace to monitor the state of samples [9, 10]. Although this kind of methods perform satisfactorily in case of highly correlated variables, they always neglect the temporal correlation between consecutive samples. Consequently, they are lean to cause a large Type-II error (i.e., fails to reject a false null-hypothesis).

To circumvent this limitation, the dynamic PCA (DPCA) [11, 12], the modified ICA (MICA) [13, 14, 15] and various other recursive MSPM methods (e.g., [16, 17, 18, 19]) have been proposed thereafter. These methods usually add time-lagged variables in a sliding window to form a data matrix that captures the (local) dynamic characteristics of the underlying process. Compared with the traditional PCA or ICA, window-based methods are easier to distinguish sample measurement from noise, thus offering a reliable avenue to address challenges associated with continuous processes [20, 21].

To further improve the performance of the above window-based methods, efficient extraction of high-order statistics of process variables is crucial [22, 23, 24, 25, 21, 26]. Notable examples include statistics pattern analysis (SPA) [20, 23], recursive transformed component statistical analysis (RTCSA) [24] and recursive dynamic transformed component statistical analysis (RDTCSA) [25]. Different from traditional PCA and DPCA that implicitly assume that the latent variables follow a multivariate Gaussian distribution, SPA integrates the skewness, the kurtosis, and various other high-order statistics of the process measurement in sliding windows to deal with non-Gaussian data, demonstrating superior performance over PCA and DPCA. However, SPA performs poorly in case of incipient faults [24]. To address this limitation, RTCSA and RDTCSA avoid dividing the projected space into principal component subspace and residual subspace. Instead, both methodologies take advantage of the full space to extract orthogonal transformed components (TCs), and evaluate a test statistic by incorporating the mean, the variance, the skewness, and the kurtosis of TCs. One should note that, the third- and forth-order information is usually beneficial to detect incipient faults [22, 20, 23, 24, 25, 21]. Although RTCSA and RDTCSA enjoy solid mathematical foundation, the TCs from a covariance matrix only capture linear relationships among different dimensions of measurement. Therefore, a reliable way to extract nonlinear statistics among different dimensions of measurements becomes a pivotal problem in fault detection [27, 28, 29].

The application of information theory on fault detection is an emerging and promising topic [30]. Although there are a few early efforts that attempt to shed light on fault detection with information-theoretic concepts, they simply employ (an approximation to) the MI to select a subset of the most informative variables to circumvent the curse of dimensionality (e.g., [31, 32, 33, 34, 35, 36]). To the best of our knowledge, there are only two exceptions that illuminate the potential of using information-theoretic concepts for fault detection, beyond the role of variable selection. Unfortunately, no specific method or statistical analysis is presented [35, 36]. Therefore, it still remains an open problem to design a fault detection method using information theory from *first principles*. The detailed contribution of this work is multi-fold:

- **Novel methodology:** We construct MI matrix to monitor the (possibly nonlinear) dynamics and the non-stationarity of fault process. A novel fault detection method, i.e., MI matrix based transformed component statistical analysis (MI-TCSA), is also developed thereafter.
- **Novel estimator:** Unlike previous information-theoretic fault detection methods which usually use the classical Shannon entropy functional that relies heavily on the precise estimation of underlying data distributions, we suggest using the recently proposed matrix-based Rényi's α -entropy functional to estimate MI values. The new estimator avoids estimation of the underlying probability density function (PDF), and is operated on the eigenspectrum of a (normalized) symmetric positive definite (SPD) matrix. This intriguing property makes the novel estimator can be easily applied to real-world complex industrial process which usually contains continuous, discrete and even mixed variables.
- **Detection accuracy:** Experiments on both synthetic data and the benchmark Tennessee Eastman process (TEP) indicate that MI-TCSA achieves comparable or slightly higher detection rates than state-of-the-art fault detection methods. Moreover, MI-TCSA enjoys significantly lower false detection rate.
- **Implementation details and reproducibility:** We elaborate the implementation details of MI-TCSA. We also illustrate the detectability of MI-TCSA using the eigenspectrum of the MI matrix. For reproducible results, we provide key functions (in MATLAB 2019a) concerning MI-TCSA in the Appendix².
- **Interpretability:** MI-TCSA can provide insights on the the exact root variables that lead to the occurrence of fault. In this sense, the result of MI-TCSA is interpretable, i.e., the practitioners know which variable or specific sensor data causes the fault.

The remainder of this paper is organized as follows. We first introduce the definition of MI matrix and present its estimation with the matrix-based Rényi's entropy functional in Section 2. We then describe our proposed MI-TCSA in Section 3, and elaborate its implementation details in Section 4. Experiments on both synthetic and TEP benchmark are performed in Section 5. We finally conclude this work and discuss future directions in Section 6.

Notations: Throughout this paper, scalars are denoted by lowercase letters (e.g., x), vectors appear as lowercase boldface letters (e.g., \mathbf{x}), and matrices are indicated by uppercase letters (e.g., X). The (i, j) -th element of X is represented by X_{ij} . If X is a square matrix, then X^{-1} denotes its inverse. I stands for the identity matrix with compatible dimensions. The i -th row of a matrix X is declared by the row vector \mathbf{x}^i , while the j -th column is indicated with the column vector \mathbf{x}_j . Moreover, superscript indicates time (or sample) index, subscript indicates variable index. For $\mathbf{x} \in \mathbb{R}^n$, the ℓ_p -norm of \mathbf{x} is defined as $\|\mathbf{x}\|_p \triangleq (\sum_{i=1}^n |x_i|^p)^{\frac{1}{p}}$.

²A full demo will be publicly available upon acceptance of this manuscript.

2. The MI Matrix: Definition and Estimation

2.1. The Definition of MI matrix

MI quantifies the nonlinear dependence between two random variables [37, 38]. Therefore, given a multivariate time series (here refers to fault process), an MI matrix (in a stationary environment) can be constructed by evaluating MI values between each pair of variables. Intuitively, the MI matrix can be viewed as a nonlinear extension of the classical covariance matrix. Specifically, the formal definition of MI matrix is given as follows.

Definition 1. Given a m -dimensional (stationary) process φ , let us denote \mathbf{x}_i ($i = 1, 2, \dots, m$) the i -th dimensional of the process measurement, then the MI matrix over φ is defined as:

$$M = \begin{bmatrix} I(\mathbf{x}_1; \mathbf{x}_1) & I(\mathbf{x}_1; \mathbf{x}_2) & \cdots & I(\mathbf{x}_1; \mathbf{x}_m) \\ I(\mathbf{x}_2; \mathbf{x}_1) & I(\mathbf{x}_2; \mathbf{x}_2) & \cdots & I(\mathbf{x}_2; \mathbf{x}_m) \\ \vdots & \vdots & \ddots & \vdots \\ I(\mathbf{x}_m; \mathbf{x}_1) & I(\mathbf{x}_m; \mathbf{x}_2) & \cdots & I(\mathbf{x}_m; \mathbf{x}_m) \end{bmatrix} \in \mathbb{R}^{m \times m}, \quad (1)$$

where $I(\mathbf{x}_i; \mathbf{x}_j)$ denotes MI between variables \mathbf{x}_i and \mathbf{x}_j .

According to Shannon information theory [39], $I(\mathbf{x}_i; \mathbf{x}_j)$ is defined over the joint probability distribution of \mathbf{x}_i and \mathbf{x}_j (i.e., $p(\mathbf{x}_i, \mathbf{x}_j)$) and their respectively marginal distributions (i.e., $p(\mathbf{x}_i)$ and $p(\mathbf{x}_j)$). Specifically,

$$\begin{aligned} I(\mathbf{x}_i; \mathbf{x}_j) &= \iint p(\mathbf{x}_i, \mathbf{x}_j) \log \left(\frac{p(\mathbf{x}_i, \mathbf{x}_j)}{p(\mathbf{x}_i)p(\mathbf{x}_j)} \right) d\mathbf{x}_i d\mathbf{x}_j \\ &= - \int \left(\int p(\mathbf{x}_i, \mathbf{x}_j) d\mathbf{x}_j \right) \log p(\mathbf{x}_i) d\mathbf{x}_i - \int \left(\int p(\mathbf{x}_i, \mathbf{x}_j) d\mathbf{x}_i \right) \log p(\mathbf{x}_j) d\mathbf{x}_j + \iint p(\mathbf{x}_i, \mathbf{x}_j) \log p(\mathbf{x}_i, \mathbf{x}_j) d\mathbf{x}_i d\mathbf{x}_j \\ &= - \int p(\mathbf{x}_i) \log p(\mathbf{x}_i) d\mathbf{x}_i - \int p(\mathbf{x}_j) \log p(\mathbf{x}_j) d\mathbf{x}_j + \iint p(\mathbf{x}_i, \mathbf{x}_j) \log p(\mathbf{x}_i, \mathbf{x}_j) d\mathbf{x}_i d\mathbf{x}_j \\ &= H(\mathbf{x}_i) + H(\mathbf{x}_j) - H(\mathbf{x}_i, \mathbf{x}_j), \end{aligned} \quad (2)$$

where $H(\cdot)$ denote the entropy and $H(\cdot, \cdot)$ denotes the joint entropy. In particular, $I(\mathbf{x}_i; \mathbf{x}_i) = H(\mathbf{x}_i)$.

Theoretically, the MI matrix is symmetric and non-negative³. Moreover, in the absence of any dependence in pairwise variables, the MI matrix reduces to a diagonal matrix with the entropy of each variable lies on the main diagonal. Interestingly, although MI matrix has been conjectured and also observed in our application to be positive semidefinite, this property is not always true theoretically [40].

³By applying the Jensen inequality, we have

$$I(\mathbf{x}_i; \mathbf{x}_j) = \iint p(\mathbf{x}_i, \mathbf{x}_j) \log \left(\frac{p(\mathbf{x}_i, \mathbf{x}_j)}{p(\mathbf{x}_i)p(\mathbf{x}_j)} \right) d\mathbf{x}_i d\mathbf{x}_j \geq -\log \left(\iint p(\mathbf{x}_i, \mathbf{x}_j) \left(\frac{p(\mathbf{x}_i)p(\mathbf{x}_j)}{p(\mathbf{x}_i, \mathbf{x}_j)} \right) d\mathbf{x}_i d\mathbf{x}_j \right) = -\log(\iint p(\mathbf{x}_i)p(\mathbf{x}_j) d\mathbf{x}_i d\mathbf{x}_j) = 0.$$

2.2. Estimate MI matrix with matrix-based Rényi's α -order entropy

Entropy measures the uncertainty in a random variable using a single scalar quantity [41, 42]. For a random sensor variable (or vector) \mathbf{x} , with probability density function (PDF) $p(\mathbf{x})$ in a finite set \mathbf{s} , a natural extension of the Shannon's differential entropy is the Rényi's α -order entropy [43]:

$$H_\alpha(\mathbf{x}) = \frac{1}{1-\alpha} \log \int_{\mathbf{s}} p^\alpha(\mathbf{x}) d\mathbf{x}. \quad (3)$$

It is well-known that, when $\alpha \rightarrow 1$, Eq. (3) reduces to the basic Shannon's differential entropy⁴ $H(\mathbf{x}) = - \int_{\mathbf{s}} p(\mathbf{x}) \log p(\mathbf{x}) d\mathbf{x}$. In this perspective, Rényi's entropy makes a one-parameter generalization to the basic Shannon definition by introducing a hyper-parameter α .

Information theory has been successfully applied to various machine learning, computer vision and signal processing tasks [41, 45]. Unfortunately, the accurate PDF estimation in Eq. (3) on continuous and complex data impedes its more widespread adoption in data driven science. This problem becomes more severe for process monitoring, since the obtained multivariate measurement may contain both discrete and continuous variables. Moreover, there is still no universal agreement on the definition of MI between discrete and continuous variables [46, 47], let alone its precise estimation. In this work, we use a novel estimator developed by Sánchez Giraldo *et al.* [48] to estimate MI values in MI matrix. Specifically, according to [45, 48], it is feasible to evaluate a quantity that resembles quantum Rényi's entropy [43] in terms of the normalized eigenspectrum of the Hermitian matrix of the projected data in reproducing kernel Hilbert space (RKHS), thus estimating the entropy directly from data without PDF estimation. For clarity, we directly give Sánchez Giraldo *et al.*'s definition on entropy and joint entropy.

Definition 2. Let $\kappa : \chi \times \chi \mapsto \mathbb{R}$ be a real valued positive definite kernel that is also infinitely divisible [49]. Given $\{\mathbf{x}_i\}_{i=1}^n \in \chi$, each \mathbf{x}_i can be a real-valued scalar or vector, and the Gram matrix K obtained from evaluating a positive definite kernel κ on all pairs of exemplars, that is $K = \kappa(\mathbf{x}_i, \mathbf{x}_j)$, a matrix-based analogue to Rényi's α -entropy for a normalized positive definite matrix A of size $n \times n$, such that $\text{tr}(A) = 1$, can be given by the following functional:

$$H_\alpha(A) = \frac{1}{1-\alpha} \log(\text{tr}(A^\alpha)) = \frac{1}{1-\alpha} \log_2 \left(\sum_{i=1}^n \lambda_i(A)^\alpha \right), \quad (4)$$

where A is the normalized version of K , i.e., $A = K/\text{tr}(K)$, and $\lambda_i(A)$ denotes the i -th eigenvalue of A .

Definition 3. Given n pairs of samples $(\mathbf{x}_i, \mathbf{y}_i)_{i=1}^n$, each sample contains two different types of measurements $\mathbf{x} \in \chi$ and $\mathbf{y} \in \gamma$ obtained from the same realization, and the positive definite kernels $\kappa_1 : \chi \times \chi \mapsto \mathbb{R}$ and $\kappa_2 : \gamma \times \gamma \mapsto \mathbb{R}$, a matrix-based analogue

⁴A simple proof by applying the L'Hôspital's rule at $\alpha = 1$ is shown in [44].

to Rényi's α -order joint-entropy can be defined as:

$$H_\alpha(A, B) = H_\alpha\left(\frac{A \circ B}{\text{tr}(A \circ B)}\right), \quad (5)$$

where $A_{ij} = \kappa_1(\mathbf{x}_i, \mathbf{x}_j)$, $B_{ij} = \kappa_2(\mathbf{y}_i, \mathbf{y}_j)$ and $A \circ B$ denotes the Hadamard product between the matrices A and B .

Given Eqs. (4)-(5), the matrix-based Rényi's α -order MI $I_\alpha(A; B)$ in analogy of Shannon's MI is given by:

$$I_\alpha(A; B) = H_\alpha(A) + H_\alpha(B) - H_\alpha(A, B). \quad (6)$$

Throughout this paper, we use the radial basis function (RBF) kernel $\kappa(\mathbf{x}_i, \mathbf{x}_j) = \exp(-\frac{\|\mathbf{x}_i - \mathbf{x}_j\|^2}{2\sigma^2})$ to obtain the Gram matrices. Obviously, Eq. (6) avoids real-valued PDF estimation and has no additional requirement on data characteristics (e.g., continuous, discrete, or mixed), which makes it has great potential in our application.

3. The MI-TCSA for Fault Detection

In this section, we present MI-TCSA, a novel fault detection method by monitoring the statistics associated with the MI matrix. Given a discrete time process $\mathbf{x} = \{\mathbf{x}^1, \mathbf{x}^2, \dots\} : \mathbf{x}^i \in \mathbb{R}^{1 \times m}$, at each time instant k , we construct a local sample matrix $X^k \in \mathbb{R}^{w \times m}$ of the following form:

$$X^k = \begin{bmatrix} \mathbf{x}^{k-w+1} \\ \mathbf{x}^{k-w+2} \\ \vdots \\ \mathbf{x}^k \end{bmatrix} = \begin{bmatrix} x_1^{k-w+1} & x_2^{k-w+1} & \dots & x_m^{k-w+1} \\ x_1^{k-w+2} & x_2^{k-w+2} & \dots & x_m^{k-w+2} \\ \vdots & \vdots & \ddots & \vdots \\ x_1^k & x_2^k & \dots & x_m^k \end{bmatrix} \quad (7)$$

$$\triangleq [\mathbf{x}_1 \mid \mathbf{x}_2 \mid \dots \mid \mathbf{x}_m] \in \mathbb{R}^{w \times m},$$

where \mathbf{x}_j ($1 \leq j \leq m$) denotes the j -th dimensional variable that is characterized by w realizations. Fig. 1 illustrates \mathbf{x}^t , \mathbf{x}_j and X . Each variable is mean centered and normalized to $[0, 1]$ to account for different value ranges [3, 4, 5, 6, 7]. Then the MI matrix M at time instant k is given by:

$$M = \begin{bmatrix} H(\mathbf{x}_1) & I(\mathbf{x}_1; \mathbf{x}_2) & \dots & I(\mathbf{x}_1; \mathbf{x}_m) \\ I(\mathbf{x}_2; \mathbf{x}_1) & H(\mathbf{x}_2) & \dots & I(\mathbf{x}_2; \mathbf{x}_m) \\ \vdots & \vdots & \ddots & \vdots \\ I(\mathbf{x}_m; \mathbf{x}_1) & I(\mathbf{x}_m; \mathbf{x}_2) & \dots & H(\mathbf{x}_m) \end{bmatrix} \in \mathbb{R}^{m \times m}. \quad (8)$$

The general idea of our method is that M contains all the nonlinear dependencies between any pairwise variables of the underlying fault process at time instant k . In a stationary environment, any quantities or statistics associated with M should remain unchanged or stable. However, the existence of an abrupt fault may affect, at least, the values of one or more entries in the MI matrix, thus altering the values of our monitored quantities or statistics extracted from MI matrix.

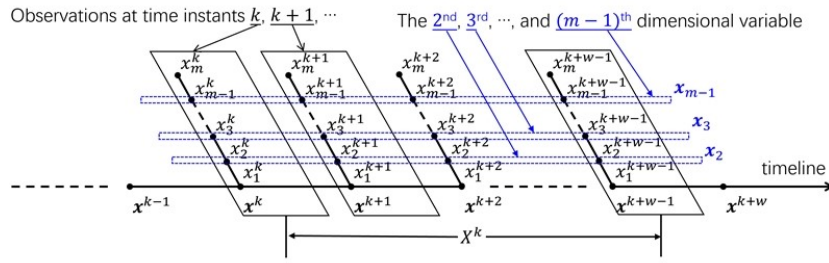


Figure 1: Local sample matrix with a sliding window of size w .

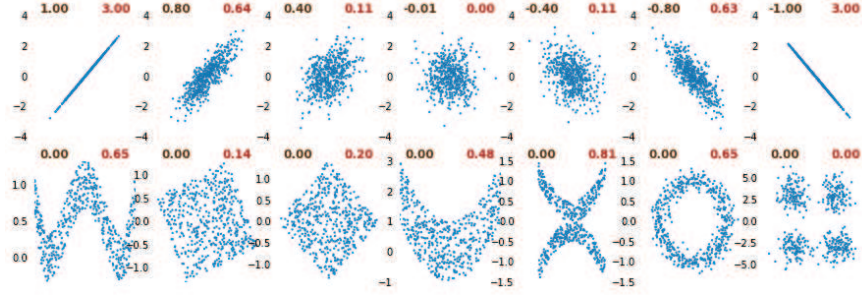


Figure 2: Examples of correlation versus mutual information (MI). Each panel illustrates a scatter plot of samples drawn from a particular bivariate distribution. For each example, the correlation between the two variables is shown in brown (left) and the MI is shown in red (right). The top row shows linear relationships, for which MI and correlation both detect a relationship. The bottom row shows a series of distributions for which the correlation is zero.

Prior art suggests that those reliable quantities can be extracted from the orthogonal space spanned by eigenvectors of the sample covariance matrix (e.g., [6, 7, 11, 50, 24, 25, 26]). Motivated by this idea, suppose the eigenvalue decomposition of MI matrix is given by $M = P\Lambda P^{-1}$, where $P \in \mathbb{R}^{m \times m}$ is the matrix of eigenvectors and $\Lambda = \text{diag}(\lambda_1, \lambda_2, \dots, \lambda_m) \in \mathbb{R}^{m \times m}$ is a diagonal matrix with eigenvalues on the main diagonal. Then, a new representation of X (denote it T) in the orthogonal space spanned by column vectors in P can be expressed as,

$$T = XP \triangleq \begin{bmatrix} \mathbf{t}^{k-w+1} \\ \mathbf{t}^{k-w+2} \\ \vdots \\ \mathbf{t}^k \end{bmatrix} \in \mathbb{R}^{w \times m}. \quad (9)$$

We term the column vectors of T the mutual information based transform components (MI-TCs). The terminology of transform components (TCs) originates from [6, 7, 24] and is defined over the sample covariance matrix $C = \frac{1}{w-1} X^T X$. Specifically, suppose P_C and Λ_C are respectively the eigenvectors and eigenvalues of C , i.e., $C = P_C \Lambda_C P_C^{-1}$, then the original TCs of X are given by $T_C = X P_C \in \mathbb{R}^{w \times m}$.

Compared with the MI matrix M , the covariance matrix C only captures the linear dependence between different dimensions of normalized measurements [24]. By contrast, the MI matrix M contains all pairwise nonlinear dependencies. Usually, the phenomenon of nonlinear dependence is common in industrial process [9, 10, 51, 24, 25, 26]. See Fig. 2 for concrete examples on the advantage of MI over linear correlation.

In each sliding window, we characterize T with a detection index $\Theta^k = [\mu_k | \nu_k | \zeta_k | \gamma_k]^T \in \mathbb{R}^{4m}$, it consists of the first-order statistic (i.e., the mean $\mu_k = \mathbb{E}(\mathbf{t}^k)$), the second-order statistic (i.e., the variance $\nu_k = \sigma_k^2 = \mathbb{E}[(\mathbf{t}^k - \mu_k)^2]$), the third-order statistic (i.e., the skewness $\zeta_k = \mathbb{E}\left[\left(\frac{\mathbf{t}^k - \mu_k}{\sigma_k}\right)^3\right]$), and the forth-order statistic (i.e., the excess kurtosis

$\gamma_k = \mathbb{E} \left[\left(\frac{\mathbf{t}^k - \mu_k}{\sigma_k} \right)^4 \right] - 3$). Specifically, the empirical estimation to μ_k , ν_k , ζ_k and γ_k are given by:

$$\mu_k = \frac{1}{w} \sum_{i=0}^{w-1} \mathbf{t}^{k-i} \in \mathbb{R}^{1 \times m}, \quad (10)$$

$$\nu_k = \frac{1}{w} \sum_{i=0}^{w-1} (\mathbf{t}^{k-i} - \mu_k)^2 \in \mathbb{R}^{1 \times m}, \quad (11)$$

$$\zeta_k = \frac{1}{w\sigma_k^3} \sum_{i=0}^{w-1} (\mathbf{t}^{k-i} - \mu_k)^3 \in \mathbb{R}^{1 \times m}, \quad (12)$$

$$\gamma_k = \frac{1}{w\sigma_k^4} \sum_{i=0}^{w-1} (\mathbf{t}^{k-i} - \mu_k)^4 - 3 \in \mathbb{R}^{1 \times m}. \quad (13)$$

Note that, $\mu^* = \mathbb{E}[\mu_k]$ (the mean of the TCs under normal condition) is used for the online calculation of detection index. When a fault occurs, one or more of the four statistics (namely, μ_k , ν_k , ζ_k and γ_k) are expected to deviate significantly from their normal values or expectations.

Given Θ^k , a similarity index for local sample matrix X^k at time instant k can be defined as:

$$D^k = \|\Theta_\sigma^{-1}(\Theta^k - \Theta_\mu)\|_p, \quad (14)$$

where Θ_μ denotes the mean value of similarity index over training data, $\Theta_\sigma = \text{diag}(\sigma_1, \sigma_2, \dots, \sigma_{4m})$ denotes a diagonal matrix in which the main diagonal consists of the standard deviation in each dimension of Θ^k . The empirical method based on training data is used to determine the upper control limit D_{cl} with a given confidence level η [20]. An online monitoring procedure is then used to quantify the dissimilarity of statistics between normal and abnormal states.

Algorithm 1 and Algorithm 2 summarize, respectively, the offline training and the online testing of our proposed MI-TCSA.

4. A Deeper Insight into the Implementation of MI-TCSA

In this section, we elaborate the implementation details of MI-TCSA. The discussion is based on a synthetic process with time-correlated dynamics[24, 25]:

$$\mathbf{x} = A\mathbf{s} + \mathbf{e}, \quad (15)$$

where $\mathbf{x} \in \mathbb{R}^m$ is the process measurements, $\mathbf{s} \in \mathbb{R}^r$ ($r < m$) is the data sources, $\mathbf{e} \in \mathbb{R}^m$ is the noise, and $A \in \mathbb{R}^{m \times r}$ is coefficient matrix that assumed to be column full rank [25, 16]. Let us assume data sources satisfy the following relations:

$$s_i^k = \sum_{j=1}^l \beta_{i,j} v_i^{k-j+1}, \quad (16)$$

Algorithm 1 MI-TCSA (training phase)

Input: Process measurements $\aleph = \{\mathbf{x}^i | \mathbf{x}^i \in \mathbb{R}^m\}_{i=1}^n$; sliding window size w ; significance level η .

Output: mean of the transform components (TCs) μ^* ; standard deviation Θ_σ of the detection index; reference mean Θ_μ of the detection index.

```
1: for  $i = 1$  to  $n$  do
2:   Construct a local time-lagged matrix  $X^i$  at time instant  $i$  by Eq. (7);
3:   Construct the MI matrix  $M^i$  by Eq. (8);
4:   Obtain the TCs  $T^i$  of  $X^i$  by Eq. (9);
5:   Obtain the detection index  $\Theta^i = [\mu_i | \nu_i | \zeta_i | \gamma_i]^T$  by Eqs. (10)-(13).
6: end for
7: Calculate the mean of the TCs  $\mu^* = \sum_{i=1}^n \mu_i$ , reference mean  $\Theta_\mu$  and standard deviation  $\Theta_\sigma$ .
8: for  $i = 1$  to  $n$  do
9:    $D^i = \|\Theta_\sigma^{-1}(\Theta^i - \Theta_\mu)\|_p$ .
10: end for
11: Determine the control limit  $D_{cl}$  at the significance level  $\eta$ .
12: return  $\mu^*$ ;  $\Theta_\sigma$ ;  $\Theta_\mu$ ;  $D_{cl}$ 
```

Algorithm 2 MI-TCSA (testing phase)

Input: The online process measurement $\{\mathbf{x}_{\text{test}}^1, \mathbf{x}_{\text{test}}^2, \dots\}$; mean of the transform components (TCs) μ^* ; standard deviation Θ_σ of the detection index; reference mean Θ_μ of the detection index; control limit D_{cl} .

Output: *Decision*: alarm or not.

```
1: while End of process not reached do
2:   Construct a local time-lagged matrix  $X_{\text{test}}^i$  at time instant  $i$  by Eq. (7);
3:   Construct the MI matrix  $M_{\text{test}}^i$  by Eq. (8);
4:   Obtain the TCs  $T_{\text{test}}^i$  of  $X_{\text{test}}^i$  by Eq. (9);
5:   Obtain the detection index  $\Theta_{\text{test}}^i = [\mu_i | \nu_i | \zeta_i | \gamma_i]^T$  with the mean of the TCs  $\mu^*$ ;
6:   Obtain the similarity index by  $D_{\text{test}}^i = \|\Theta_\sigma^{-1}(\Theta_{\text{test}}^i - \Theta_\mu)\|_p$ ;
7:   if  $D_{\text{test}}^i \geq D_{cl}$  then
8:     Alarm the occurrence of fault;
9:   else
10:     $i = i + 1$ ; Go back to Step 2.
11:   end if
12: end while
13: return Decision
```

where s_i^k is the i -th variable at time k , v_i^{k-j+1} represents the value of the i -th Gaussian data source with time independence at time $k-j+1$, $\beta_{i,j}$ denotes the weight coefficient, $l \geq 2$. Obviously, both \mathbf{s} and \mathbf{x} are time-correlated.

Here, the fault type of sensor bias⁵ is considered:

$$\mathbf{x}^* = \mathbf{x} + \mathbf{f}, \quad (17)$$

where \mathbf{x}^* is the measurement under sensor bias, and \mathbf{x} denotes the fault-free portion. In the following, we will show how \mathbf{f} affects the matrix-based Rényi's α -order entropy.

The matrix-based Rényi's α -order entropy is a non-parametric measure of entropy. For the p -th variable with w realizations, we build its Gram matrix $K \in \mathbb{R}^{w \times w}$ (at time instant k) by projecting it into a RKHS with an infinite divisible kernel⁶:

$$K_{\mathbf{x}_p} = \begin{bmatrix} 1 & \exp\left(-\frac{(x_p^{k-w+1}-x_p^{k-w+2})^2}{2\sigma^2}\right) & \cdots & \exp\left(-\frac{(x_p^{k-w+1}-x_p^k)^2}{2\sigma^2}\right) \\ \exp\left(-\frac{(x_p^{k-w+2}-x_p^{k-w+1})^2}{2\sigma^2}\right) & 1 & \cdots & \exp\left(-\frac{(x_p^{k-w+2}-x_p^k)^2}{2\sigma^2}\right) \\ \vdots & \vdots & \ddots & \vdots \\ \exp\left(-\frac{(x_p^k-x_p^{k-w+1})^2}{2\sigma^2}\right) & \exp\left(-\frac{(x_p^k-x_p^{k-w+2})^2}{2\sigma^2}\right) & \cdots & 1 \end{bmatrix}. \quad (18)$$

We normalize K by its trace, i.e., $K = K/\text{tr}(K)$. It should be noted that the kernel induced mapping can be understood as a means of computation of high order statistics⁷.

Suppose the fault occurs exactly at the p -th variable, i.e., $\mathbf{x}_p^* = \mathbf{x}_p + \mathbf{f}$ and $\mathbf{f} = \{f^{k-w+1}, f^{k-w+2}, \dots, f^k\}$. The (i, j) -th entry of the Gram matrix K associated with \mathbf{x}_p becomes:

$$\begin{aligned} \exp\left(-\frac{\|\mathbf{x}_p^{i*} - \mathbf{x}_p^{j*}\|^2}{2\sigma^2}\right) &= \exp\left(-\frac{[(x_p^i + f^i) - (x_p^j + f^j)]^2}{2\sigma^2}\right) \\ &= \exp\left(-\frac{[(x_p^i - x_p^j) + (f^i - f^j)]^2}{2\sigma^2}\right) \\ &= \exp\left(-\frac{(x_p^i - x_p^j)^2}{2\sigma^2}\right) \exp\left(-\frac{(x_p^i - x_p^j)(f^i - f^j)}{\sigma^2}\right) \exp\left(-\frac{(f^i - f^j)^2}{2\sigma^2}\right), \end{aligned} \quad (19)$$

⁵Other fault types, such as sensor precision degradation $\mathbf{x}^* = \eta\mathbf{x}$, gain degradation $\mathbf{x}^* = \mathbf{x} + \xi_m \mathbf{e}^{[s]}$, additive process fault $\mathbf{x} = A(\mathbf{s} + \xi_m \mathbf{f}^{[p]}) + \mathbf{e}$ and dynamic changes $\beta = \beta + \Delta\beta$ can also be analyzed similarly.

⁶In this work, we simply use the radial basis function (RBF) kernel $G_\sigma(\cdot) = \exp(-\frac{\|\cdot\|^2}{2\sigma^2})$ as recommended in [48, 45].

⁷By the Taylor expansion of the RBF kernel, we have $\kappa(x^i, x^j) = \exp(-\gamma\|x^i - x^j\|^2) = \exp(-\gamma x^{i2}) \exp(-\gamma x^{j2}) \left(1 + \frac{2\gamma x^i x^j}{1!} + \frac{(2\gamma x^i x^j)^2}{2!} + \frac{(3\gamma x^i x^j)^2}{3!} + \dots\right)$, where $\gamma = \frac{1}{2\sigma^2}$.

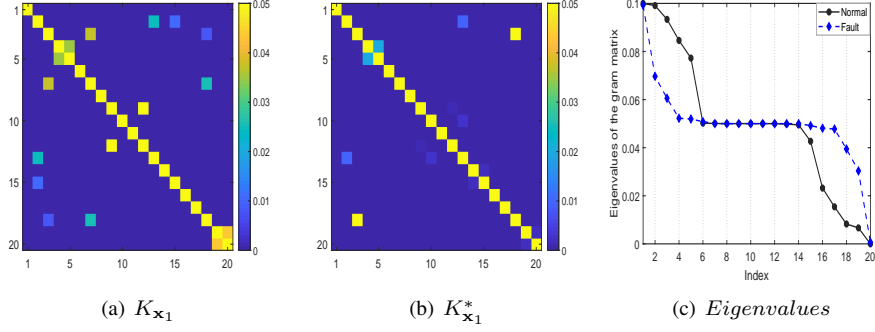


Figure 3: The (normalized) Gram matrices and their eigenspectrum: (a) $K_{\mathbf{x}_1}$ in normal state; (b) $K_{\mathbf{x}_1}^*$ in fault state; (c) the eigenspectrum of $K_{\mathbf{x}_1}$ and $K_{\mathbf{x}_1}^*$.

where i, j are time indices. Therefore, the new Gram matrix $K_{\mathbf{x}_p}^*$ can be represented as:

$$K_{\mathbf{x}_p}^* = K_{\mathbf{x}_p} \circ K_{\langle \mathbf{x}_p, \mathbf{f} \rangle} \circ K_{\mathbf{f}}, \quad (20)$$

where

$$K_{\langle \mathbf{x}_p, \mathbf{f} \rangle} = \begin{bmatrix} 1 & \exp\left(-\frac{(x_p^{k-w+1}-x_p^{k-w+2})(f^{k-w+1}-f^{k-w+2})}{\sigma^2}\right) & \cdots & \exp\left(-\frac{(x_p^{k-w+1}-x_p^k)(f^{k-w+1}-f^k)}{\sigma^2}\right) \\ \exp\left(-\frac{(x_p^{k-w+2}-x_p^{k-w+1})(f^{k-w+2}-f^{k-w+1})}{\sigma^2}\right) & 1 & \cdots & \exp\left(-\frac{(x_p^{k-w+2}-x_p^k)(f^{k-w+2}-f^k)}{\sigma^2}\right) \\ \vdots & \vdots & \ddots & \vdots \\ \exp\left(-\frac{(x_p^k-x_p^{k-w+1})(f^k-f^{k-w+1})}{\sigma^2}\right) & \exp\left(-\frac{(x_p^k-x_p^{k-w+2})(f^k-f^{k-w+2})}{\sigma^2}\right) & \cdots & 1 \end{bmatrix}, \quad (21)$$

and

$$K_{\mathbf{f}} = \begin{bmatrix} 1 & \exp\left(-\frac{(f^{k-w+1}-f^{k-w+2})^2}{2\sigma^2}\right) & \cdots & \exp\left(-\frac{(f^{k-w+1}-f^k)^2}{2\sigma^2}\right) \\ \exp\left(-\frac{(f^{k-w+2}-f^{k-w+1})^2}{2\sigma^2}\right) & 1 & \cdots & \exp\left(-\frac{(f^{k-w+2}-f^k)^2}{2\sigma^2}\right) \\ \vdots & \vdots & \ddots & \vdots \\ \exp\left(-\frac{(f^k-f^{k-w+1})^2}{2\sigma^2}\right) & \exp\left(-\frac{(f^k-f^{k-w+2})^2}{2\sigma^2}\right) & \cdots & 1 \end{bmatrix}. \quad (22)$$

In case of incipient faults, $f^i - f^j \approx 0$, Eq. (22) reduces to an all-ones matrix. As a result, Eq. (20) can be approximated with $K_{\mathbf{x}_p}^* \approx K_{\mathbf{x}_p} \circ K_{\langle \mathbf{x}_p, \mathbf{f} \rangle}$. Take the simulation data described in section 5.1 as an example, \mathbf{f} is induced on \mathbf{x}_1 , the Gram matrix of \mathbf{x}_1 and \mathbf{x}_1^* are shown in Fig. 3. As can be seen, the incipient fault \mathbf{f} causes minor changes on the (normalized) Gram matrix as well as its eigenspectrum, and thus the entropy of the variable.

We now discuss the change of MI between the p -th variable \mathbf{x}_p and the q -th variable \mathbf{x}_q . Again, suppose the fault of sensor bias occurs at the p -th variable \mathbf{x}_p^* , the difference

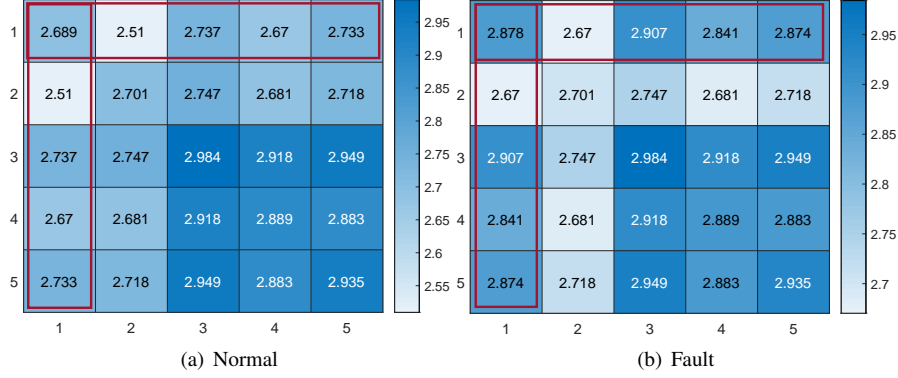


Figure 4: The MI matrix under (a) normal state; and (b) fault state. The entries with changed values are marked with red rectangles.

between $I(\mathbf{x}_p; \mathbf{x}_q)$ and $I(\mathbf{x}_p^*; \mathbf{x}_q)$ is:

$$\begin{aligned}
\Delta I(\mathbf{x}_p^*; \mathbf{x}_q) &= I(\mathbf{x}_p^*; \mathbf{x}_q) - I(\mathbf{x}_p; \mathbf{x}_q) \\
&= [H_\alpha(A_p^*) + H_\alpha(A_q) - H_\alpha(A_p^*, A_q)] - [H_\alpha(A_p) + H_\alpha(A_q) - H_\alpha(A_p, A_q)] \\
&= H_\alpha(A_p^*) - H_\alpha(A_p^*, A_q) - H_\alpha(A_p) + H_\alpha(A_p, A_q) \\
&= \frac{1}{1 - \alpha} \log_2 \left(\frac{\sum_{i=1}^w \lambda_i(A_p^*)^\alpha \sum_{i=1}^w \lambda_i \left(\frac{A_p \circ A_q}{\text{tr}(A_p \circ A_q)} \right)^\alpha}{\sum_{i=1}^w \lambda_i(A_p)^\alpha \sum_{i=1}^w \lambda_i \left(\frac{A_p^* \circ A_q}{\text{tr}(A_p^* \circ A_q)} \right)^\alpha} \right),
\end{aligned} \tag{23}$$

where $\lambda_i(A)$ denotes the i -th eigenvalue of matrix A , the normalized Gram matrix obtained from the corresponding variable.

Again, we use the simulated data described in section 5.1 as an example, where the fault is induced in \mathbf{x}_1 . By comparing the MI matrix under normal and fault states, as shown in Fig. 4, we can observe that all entries related to \mathbf{x}_1 have a sudden change. The result also indicates that our methodology has the potential to identify the exact fault sources, which makes our detection result interpretable.

5. Experiments

In this section, experiments on both synthetic data and the real-world Tennessee Eastman process (TEP) are conducted to demonstrate the superiority of our proposed MI-TCSA over state-of-the-art fault detection methods. We also evaluate the robustness of MI-TCSA with respect to different hyper-parameter settings.

Two generally used metrics, namely the fault detection rate (FDR) and the false alarm rate (FAR), are employed for performance evaluation[1, 52, 53]. The FDR is the

probability of event where an alarm is raised when a fault really occurs,

$$\text{FDR} = \text{prob}(D > D_{\text{cl}} | \text{fault} \neq 0), \quad (24)$$

where D and D_{cl} are respectively the similarity index and its corresponding control limit. By contrast, the FAR is the percentage of the samples under normal state but are identified as faults,

$$\text{FAR} = \text{prob}(D > D_{\text{cl}} | \text{fault} = 0). \quad (25)$$

Obviously, a higher FDR and a lower FAR is expected.

5.1. Numerical Simulation

Motivated by [16, 24, 25], we consider a multivariate nonlinear process generated by the following equation:

$$\begin{bmatrix} x_1 \\ x_2 \\ x_3 \\ x_4 \\ x_5 \end{bmatrix} = \begin{bmatrix} 0.2183 & -0.1693 & 0.2063 \\ -0.1972 & 0.2376 & 0.1736 \\ 0.9037 & -0.1530 & 0.6373 \\ 0.1146 & 0.9528 & -0.2624 \\ 0.4173 & -0.2458 & 0.8325 \end{bmatrix} \begin{bmatrix} s_1^2 \\ s_2 s_3 \\ s_3^3 \end{bmatrix} + \begin{bmatrix} e_1 \\ e_2 \\ e_3 \\ e_4 \\ e_5 \end{bmatrix}, \quad (26)$$

where s satisfies $s_i^k = \sum_{j=1}^l \beta_{i,j} v_i^{k-j+1}$ with a weight matrix β given by,

$$\beta = \begin{bmatrix} 0.6699 & 0.0812 & 0.5308 & 0.4527 & 0.2931 \\ 0.4071 & 0.8758 & 0.2158 & -0.0902 & 0.1122 \\ 0.3035 & 0.5675 & 0.3064 & 0.1316 & 0.6889 \end{bmatrix},$$

v denotes three mutually independent Gaussian distributed data sources with mean of $[0.3, 2.0, 3.1]^T$ and standard deviation of $[1.0, 2.0, 0.8]^T$, and e denotes Gaussian white noises with standard deviation $[0.061, 0.063, 0.198, 0.176, 0.170]^T$. Same to [24, 25], we consider four different types of faults that cover a broad spectrum of real-life scenarios,

- Type I: Sensor bias $\mathbf{x}^* = \mathbf{x} + f$, with $f = 5.6 + \mathbf{e}$, \mathbf{e} randomly chose from $[0, 1.0]$;
- Type II: Sensor precision degradation $\mathbf{x}^* = \eta \mathbf{x}$ with $\eta = 0.6$;
- Type III: Additive process fault $\mathbf{s}^* = \mathbf{s} + f$ with $f = 1.2$;
- Type IV: Dynamic changes $\tilde{\beta} = \beta + \Delta\beta$ with $\Delta\beta_3 = [-0.825, 0.061, 0.662, -0.820, 0.835]$, where β_3 denotes the 3-th row of β .

The training set contains 10,000 samples, the testing set contains 4,000 samples. All the faults are introduced after the 1,000-th sample. For convenience, we assume sensor fault occurs at \mathbf{x}_1 (i.e., the first dimension of observable measurement), and process fault occurs at \mathbf{s}_1 (i.e., the first independent data sources). Empirical evaluation aims to answer the following three questions:

- Can MI manifest more complex dependence among different dimensions of measurement than the classical correlation coefficient?
- Is MI-TCSA robust to hyper-parameter settings and how hyper-parameters affect the performance of MI-TCSA?
- Does MI-TCSA outperform existing state-of-the-art window-based fault detection methods?

5.1.1. MI versus Pearson's correlation coefficient

Firstly, we demonstrate the advantage of MI over the Pearson's correlation coefficient γ on manifesting the linear or nonlinear dependencies between two variables. Intuitively, if two random variables are linearly correlated, we can obtain both high γ^2 and MI values. However, if they are nonlinearly correlated, we can only obtain high MI value but small γ^2 [32]. Therefore, MI should always be a superior metric to measure the degree of interactions than Pearson's correlation coefficient. We perform a simple simulation to support our argument.

Specifically, we focus on the first 4,000 samples in the training set and compute both MI and γ^2 in each window data of size 100. We finally obtain 3,601 pairs of MI and γ^2 . We evaluate MI with both the basic Shannon's discrete entropy functional and our suggested matrix-based Rényi's α -order entropy functional. In case of Shannon entropy, we discretize continuous variables into 5 bins of equal width to estimate the underlying distributions. The values of MI (y axis) and γ^2 (x axis) are plotted in Fig. 5. As can be seen, there are strong nonlinear dependencies in our simulated data. Take Fig. 5(b) as an example, when $\gamma^2 = 0.6$, the smallest MI is 0.33. This indicates that there is strong (linear) dependence in the area of $I \in [0.33, 1.2]$, and $\gamma^2 \in [0.6, 1.0]$. However, the existence of multiple points in the area $I \in [0.33, 1.2]$ and $\gamma^2 \in [0.4, 0.6]$ suggests that some variables contain strong nonlinear dependencies that can only be quantified by MI. Moreover, one should note that, there are almost no points in the area that $I \in [0, 0.33]$ and $\gamma^2 \in [0.6, 1.0]$. In other words, all dependencies detected by correlation coefficient can also be captured by MI.

Further, to quantitatively demonstrate the superiority of MI matrix over the well-known covariance matrix on nonlinear fault detection, we use MI matrix as a substitute to the covariance matrix in the basic PCA-based fault detection approach. We denote this simple modification as MI-PCA. Both Hotelling T^2 and squared prediction error (SPE) are considered for PCA and MI-PCA, shown in Fig. 6. In case of T^2 , MI-PCA always has higher or almost the same FDR values, but significantly smaller FAR values. In case of SPE, although traditional PCA has smaller FAR, its results are meaningless. In fact, if we look deeper, the FDR of PCA is almost zero, which suggests that traditional PCA completely fails.

5.1.2. Hyperparameter analysis

We then present a comprehensive analysis on the effects of three hyper-parameters, namely the entropy order α , the kernel size σ and the length w of sliding window in MI-TCSA. We focus our discussion on the process data with time-correlated dynamic changes, i.e., fault Type V. The FDR and FAR values of our methodology with respect to different hyper-parameter settings are shown in Fig. 7, Fig. 8 and Fig. 9.

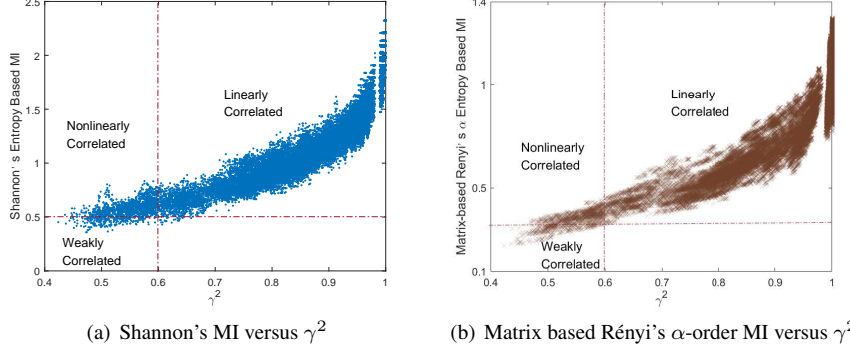


Figure 5: The comparison between Pearson's correlation coefficient γ^2 with (a) Shannon MI; and (b) matrix based Rényi's α -order MI.

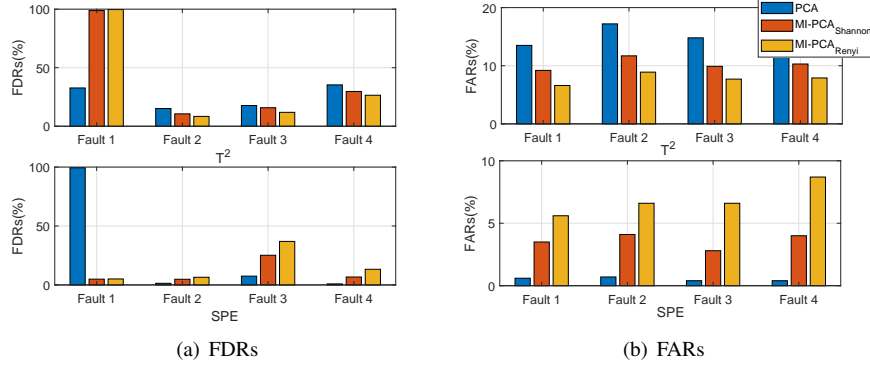


Figure 6: Performance comparison between PCA and MI-PCA in terms of FDR (the larger the better) and FAR (the smaller the better). We replace the covariance matrix in the basic PCA-based fault detection with MI matrix estimated with both Shannon entropy (denote it MI-PCA_{Shannon}) and matrix based Rényi's α -order entropy (denote it MI-PCA_{Rényi}). We use both Hotelling T^2 and squared prediction error (SPE) to monitor the state of samples.

The choice of α is associated with the task goal. If the application requires emphasis on tails of the distribution (rare events) or multiple modalities, α should be less than 2, but if the goal is to characterize modal behavior, α should be greater than 2. $\alpha = 2$ provides neutral weighting [45, 54]. The detection performances of different values of α (we use both ℓ_∞ and ℓ_2 in Eq. (14)) are presented in Fig. 7. As can be seen, the FDR values are always larger than 99.5%, which suggests that FDR is less sensitive to the changes of α . On the other hand, the FAR keeps a stable value in the range $\alpha \in [0.5, 1.2]$, but suddenly increases to 25% or above when $\alpha \geq 2$. Therefore, we recommend α in the range $[0.5, 1.2]$ for MI-TCSA.

The parameter σ controls the locality of the estimator, its selection can follow Silverman's rule of thumb for density estimation [55] or other heuristics from a graph cut perspective (e.g., the 10 to 30 percent of the total range of the Euclidean distances between all pairwise data points [56]). For example, the range from a graph cut per-

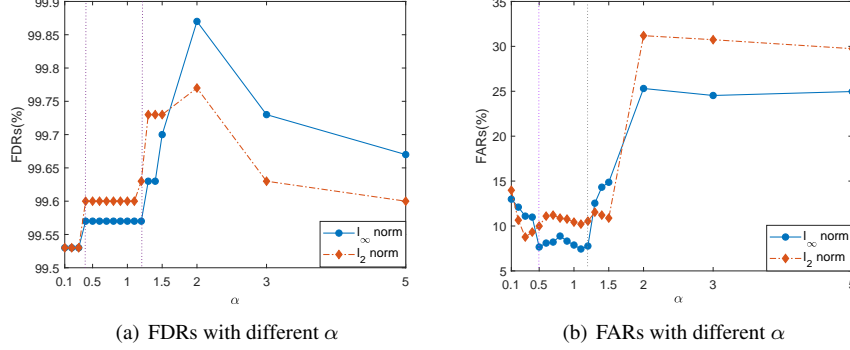


Figure 7: Detection performances of different α , both ℓ_∞ and ℓ_2 norm are considered in the calculation of similarity index D . The commonly used window size 100 is chosen here.

spective corresponds to $0.21 < \sigma < 1.33$ on the normalized data. According to Fig. 8, FDR is always larger than 99.20%, whereas FAR is relatively more sensitive to σ . Specifically, FAR reaches to its minimum value when σ is around 0.5. After that, FAR is consistently increasing when $\sigma \in [1, 100]$. To achieve higher FDR and lower FAR values, we thus recommend σ in the range $[0.4, 1]$ for MI-TCSA.

Increasing the size of sliding window reduces the variations in corresponding entries in consecutive MI matrices, thus is prone to produce a more stable distribution of their eigenspectrum. However, a smaller sliding window w would break the stationarity assumption in our methodology, which leads to poor fault detection capability in the transition phase and an unacceptable detection delay. According to Fig. 9, FDR remains stable when $w \in [50, 120]$, and decreases as the window length increasing when $w \geq 120$. By contrast, FAR is more sensitive to w than FDR, but its changing patterns are not consistent for ℓ_2 norm and ℓ_∞ norm. We choose $w = 100$ in the following experiments, because it can strike a good trade-off between FDR and FAR for both ℓ_2 norm and ℓ_∞ norm.

5.1.3. Comparison with state-of-the-art methods

We compare our proposed MI-TCSA with four state-of-the-art window based data-driven fault detection approaches, namely DPCA [11], SPA [20], RTCSA [24] and RDTCSA [25]. The hyperparameters of MI-TCSA are set to $\alpha = 1.01$, $\sigma = 0.5$ and $w = 100$. For DPCA, 90% cumulative percent variance is used to determine the number of principle components. For RTCSA, RDTCSA and MI-TCSA, their detection performances are illustrated in Table 1 and Table 2.

According to Table 1, MI-TCSA can effectively detect different types of faults and has the highest detection rate. Our advantage becomes more obvious for fault Type III and fault Type V, namely the additive process fault and dynamic changes. Moreover, as demonstrated in Table 2, for each test process, MI-TCSA achieves smaller FAR values at the early stage of the normal phase. Although SPA achieves nearly zero FAR values, its FDR values is too small, which indicates that SPA is hard to identify faults here. This is not hard to understand. Note that SPA uses a time lag of 1. In this sense, any

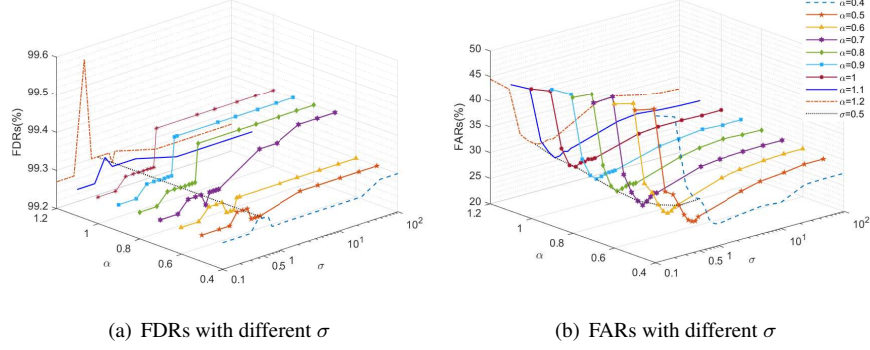


Figure 8: Detection performances of different σ , $\sigma \in \{0.1, 0.2, 0.3, 0.4, 0.5, 0.6, 0.7, 0.8, 0.9, 1, 5, 10, 24, 50, 100\}$, displayed in exponential axis. ℓ_2 norm is considered in the calculation of similarity index D .

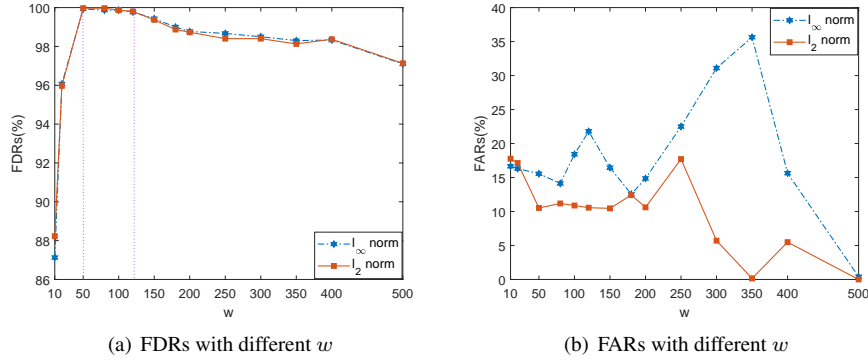


Figure 9: Detection performances of different w , both ℓ_∞ and ℓ_2 norm are considered for scalarization in the calculation of similarity index D .

Table 1: The FDRs of different methods for the numerical simulations

FDR (%)	DPCA		SPA		RTCSA	RDTCSA	MI-TCSA
	T^2	SPE	D_r	D_p			
1	51.17	99.70	0.80	2.80	88.43	91.01	91.57
2	21.23	21.0	2.40	6.67	82.50	100	99.63
3	33.10	99.83	0.77	7.37	96.60	96.83	97.50
4	81.23	85.57	29.13	99.13	99.70	99.70	99.87
Aver.	46.68	76.53	8.28	29.0	91.81	96.89	97.14

T^2 denotes Hotelling's T^2 statistic; SPE denotes squared prediction error; D_r and D_p denote SPE and T^2 of statistics patterns (SPs) in SPA framework, respectively. For SPA, the selected statistics are mean, variance, skewness, and kurtosis. For DPCA, SPA and RDTCSA, the time lag is set to 2, 1 and 1 respectively. The window lengths are all set as the commonly used 100. For RTCSA, RDTCSA and MITCSA, ℓ_2 norm is used as scalarization. The significance level is set as 5%.

Table 2: The FARs of different methods for the numerical simulations

FAR (%)	DPCA		SPA		RTCSA	RDTCSA	MI-TCSA
	T^2	SPE	D_r	D_p			
1	17.31	18.28	0.22	10.32	6.22	3.11	1.78
2	20.20	19.44	0	0	4.67	1.44	5.01
3	18.28	15.53	0	9.54	4.88	3.65	2.77
4	19.44	17.92	0	15.54	11.88	15.53	2.77
Aver.	18.81	17.79	0.055	8.85	6.91	5.93	3.08

two adjacent windows of data only differ in 1 sample. The highly overlapped windows will lead to highly correlated SPs, which severely deteriorate the capability of SPA [20].

5.2. TEP Experiment

As a public benchmark of chemical industrial process, TEP is designed to provide an actual industrial process for evaluating process control approaches [57, 58]. It has been widely used for multivariable process control problems. In this application, we use the simulation data generated by the closed-loop Simulink models developed by Braatz [58, 59, 60] to evaluate the effectiveness of our proposed MI-TCSA. We use 22 continuous process measurements and 11 manipulated variables for monitoring, which constitutes 33 dimensional of input data. To obtain a reliable significance level, we generate 200 hours of training data (4,000 samples in total) and 100 hours of testing data (2,000 samples in total). In each test data, a fault occurs exactly after 20 hours from the beginning.

First, the MI matrix of normal state, fault 1 (step fault) and fault 14 (sticking fault) are shown in Fig. 10. Obviously, the MI matrix keeps almost the same in different time instants under the normal state. However, the occurrence of a fault will lead to different joint or marginal distributions on each dimensional of input, and thus change the entry values in MI matrix. Moreover, different types of faults produce different changes of MI matrix.

The mean of MI values between one variable and all remaining variables⁸ are shown in Fig. 11. As Fig. 11(a) shown, the central box becomes wider and the 75-th percentiles becomes larger. This indicates that the fault 1 is possibly a step change. In fact, fault 1 indeed induce a step change on stream 4. This feeding changes of reactants A, B and C causes a global impacts on measurements. By contrast, fault 14 induces a sticking change on the reactor cooling water valve, and the most relevant variables are in dimensions 9, 21 and 32 [59]. From Fig. 11(b), there are indeed three outliers which are plotted individually using the “+” symbol, corresponding to the 9-th, 21-th and 32-th dimensional variables. In other words, the changes on the dimensions 9, 21 and 32 are exactly the driving force that lead to the changes in MI matrix (and hence its eigenspectrum). In this sense, our MI-TCSA also provides insights on the exact root variables that cause the fault, i.e., our MI-TCSA is interpretable. One should also note

⁸For the i -th variable, we just compute the mean of $I(\mathbf{x}_1, \mathbf{x}_i), \dots, I(\mathbf{x}_{i-1}, \mathbf{x}_i), I(\mathbf{x}_{i+1}, \mathbf{x}_i), \dots, I(\mathbf{x}_m, \mathbf{x}_i)$.

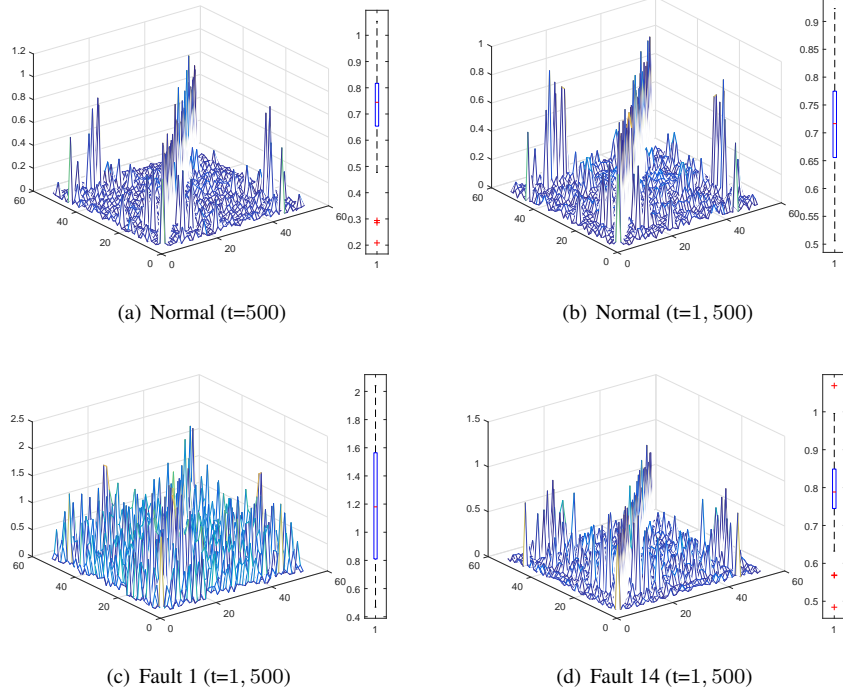


Figure 10: The MI matrix of TEP under normal and fault states. (a) The MI matrix of normal state at 500-th sampling instant. (b) The MI matrix of normal state at 1,500-th sampling instant. (c) The MI matrix of fault 1 at 1,500-th sampling instant. (d) The MI matrix of fault 14 at 1,500-th sampling instant.

that, an interpretable results also benefit problems related to fault isolation [61] and restoration [62].

Next, we use the empirical method to determine the confidence limits of different MSPM methods under the same confidence level. Without loss of generality, the window lengths of all competing methods are set to 100, and all the statics mentioned in Section 3 are used here. The average FDR and FAR values of different MSPM methods on TEP are summarized in Table 3 and Table 4, respectively.

It can be observed from Table 3 that the FDR of RTCSA, RDTCSA, and MI-TCSA are consistently higher than other methods and remain stable across different types of faults. Moreover, our MI-TCSA always outperforms RTCSA, owing to the superiority of MI over covariance matrix in capturing the intrinsic interactions (either linear or non-linear) between pairwise variables. MI-TCSA detects most of faults. Although our method has relatively lower FDR on step fault 5 and unknown fault 19 with $w = 100$, its detection performance in both faults can be significantly improved with larger window size w (see Fig. 12).

From Table 4 all the methods achieve favorable FAR, approaching to the theoretical minimum value, i.e., the used significance level. Moreover, our FAR is lower than RTCSA and RDTCSA. This result confirms the superiority of MI in capturing the in-

Table 3: The FDRs of different MSPM methods for TEP

FDR (%)	Fault Type	DPCA		SPA		RTCSA	RDTCSA	MI-TCSA
		T^2	SPE	D_r	D_p			
1	Step	99.91	99.94	99.88	99.81	99.62	99.56	99.69
2	Step	99.19	98.88	99.12	99.12	98.50	98.69	98.31
4	Step	11.63	100	16.50	100	98.38	99.44	99.56
5	Step	14.94	28.56	19.50	87.81	99.88	97.25	77.38
6	Step	99.50	100	13.63	13.63	100	99.94	100
7	Step	100	100	44.12	100	100	100	100
8	Random	98.88	93.63	99.12	99.12	97.88	97.75	98.62
10	Random	21.69	51.62	59.56	88.12	96.63	37.38	96.06
11	Random	36.88	95.44	99.69	100	96.25	92.94	99.0
12	Random	99.38	97.31	99.31	99.31	99.38	99.50	100
13	Slow drift	98.56	92.31	98.31	100	97.88	98.0	98.25
14	Sticking	99.88	99.94	99.94	99.94	99.88	99.88	99.88
16	Unknown	15.37	52.38	63.56	91.81	99.75	79.31	99.50
17	Unknown	87.19	98.31	98.0	99.31	97.81	97.75	97.88
18	Unknown	94.56	95.75	93.81	95.56	93.75	93.69	94.69
19	Unknown	48.25	49.75	29.38	99.62	100	97.19	78.19
20	Unknown	47.38	61.31	96.19	96.75	96.69	95.81	96.31

The window lengths are all set as 100. The selected statistics are mean, variance, skewness, and kurtosis. For RTCSA, RDTCSA and MITCSA, ℓ_∞ norm is used as scalarization. For DPCA and RDTCSA, the time lag is set to 2 and 1 respectively, recommended by authors [24, 25]. The significance level is set as 2%.

Table 4: The average FARs of different MSPM methods for TEP

FAR (%)	DPCA		SPA		RTCSA	RDTCSA	MI-TCSA
	T^2	SPE	D_r	D_p			
Normal	2.05	3.95	4.73	5.96	2.89	3.63	1.18

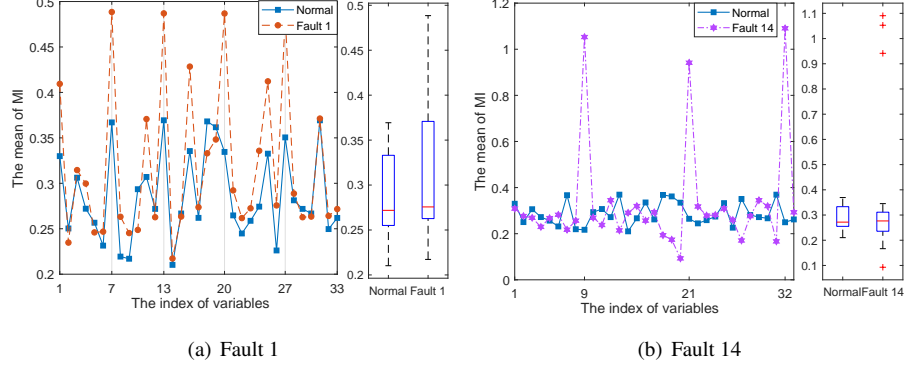


Figure 11: The means of MI matrix of TEP under fault states. The left plot is the means of MI along each variable, and the right is their confidence interval. (a) Fault 1. (b) Fault 14.

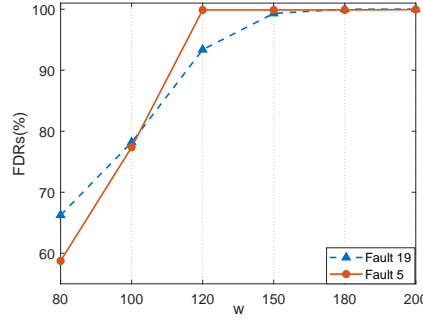


Figure 12: Detection performances of different w for fault 5 and 19 in TEP.

trinsic interactions. On the other hand, the detection delay is inevitable owing to the use of sliding windows, a common drawback of the window-based MSPM methods. Take fault 1 for instance, detection performances of RTCSA, RDTCSA and MI-TCSA are illustrated in Fig. 13. Our proposed MI-TCSA has the lowest FAR, and its time delay is only 4 samples, which indicates that MI-TCSA is more sensitive to fault 1 than RTCSA. Because RDTCSA uses a time lag, it has lower FDR than MI-TCSA in the transition phase.

6. Conclusion

This work presents a novel way to use information theory on fault detection. Before our work, most of the information-theoretic fault detection methods just use mutual information (MI) as a dependence measure to select the most informative dimensions to circumvent the curse of dimensionality. Distinct from these efforts, our method does not perform feature selection. Instead, we construct a MI matrix to quantify all non-linear dependencies between pairwise dimensional of data. We demonstrated that the

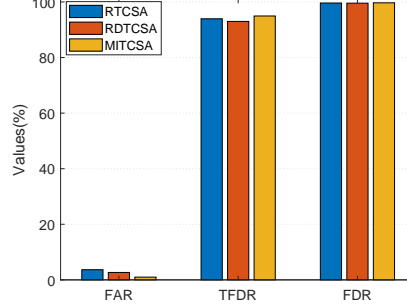


Figure 13: Detection performances of TCSA methods for fault 1 in TEP. TFDR refers to the FDR value in the transition phase. The higher TFDR, the better performance of the used methodology.

MI matrix can identify the root variables that cause the fault, and that the transformed components extracted from MI matrix enables an early detection of faults. We also demonstrated that the matrix-based Rényi's α -order entropy enables an efficient estimation of MI in complex fault process. Simulations of both synthetic data and the benchmark TEP indicate our proposed methodology can achieve almost the same or slightly higher fault detection rate (FDR), but the lowest false alarm rate (FAR). We also present a thorough analysis on the parameter setting of our methodology, especially how those parameters control the trade-off between FAR and FDR.

Finally, one should note that the mutual information matrix is a powerful tool to analyze the interactions in multivariate time series in signal processing, economics and various engineering applications. Unfortunately, most of its properties, characteristics, and practical advantages are still largely unknown. This work is a first step to understand the value of nonparametric dependence measures (especially the mutual information matrix) in monitoring industrial process. We will continue working along this direction to improve the performance of our method and also theoretically explore its fundamental properties.

Acknowledgment

This work was supported by the National Natural Science Foundation of China under Grant 61751304, 61933013; and the Henan Provincial Science and Technology Research Foundation of China under Grant 202102210125.

Appendix

For reproducible results, we provide key functions (in MATLAB 2019a) of the proposed MI-TCSA. Specifically, “mutual_information_estimation.m” estimates the matrix-based Rényi's α -order mutual information (Eq. 6), in which the “gaussianMatrix.m” evaluates the kernel induced Gram matrix (Eq. 18). “MI_matrix.m” obtains a series of mutual information matrix at each time instant k . “MITCSA.m” computes the similarity index (Eq. 14).

```

1 function mutual_information = mutual_information_estimation(variable1,
    variable2,sigma,alpha)
2 % variable 1 is i-th dimensional of the process measurement (i-th
    variable)
3 % variable 2 is j-th dimensional of the process measurement (j-th
    variable)
4 %% estimate entropy for variable 1
5 K_x = real(guassianMatrix(variable1,sigma))/size(variable1,1);
6 [~, L_x] = eig(K_x);
7 lambda_x = abs(diag(L_x));
8 H_x = (1/(1-alpha))*log((sum(lambda_x.^alpha)));
9
10 %% estimate entropy for variable 2
11 K_y = real(guassianMatrix(variable2,sigma))/size(variable2,1);
12 [~, L_y] = eig(K_y);
13 lambda_y = abs(diag(L_y));
14 H_y = (1/(1-alpha))*log((sum(lambda_y.^alpha)));
15
16 %% estimate joint entropy H(X,Y)
17 K_xy = K_x.*K_y.*size(variable1,1);
18 [~,L_xy] = eig(K_xy);
19 lambda_xy = abs(diag(L_xy));
20 H_xy = (1/(1-alpha))*log( (sum(lambda_xy.^alpha)));
21
22 %% estimate mutual information I(X;Y)
23 mutual_information = H_x + H_y - H_xy;
24
25 end

```

```

1 function K = gaussianMatrix(X,sigma)
2 G = X*X';
3 K = bsxfun(@minus, 2*G, diag(G)');
4 K = exp((1/(2*sigma^2))*bsxfun(@minus, K, diag(G)));
5
6 end

```

```

1 function MImatrixcell = MI_matrix(data,sigma,alpha,MIsiZe)
2 % Input:
3 %     data is the sample matrix X
4 %     MIsiZe is the length of sliding window
5 %     alpha is the entropy order
6 %     sigma is the kernel size
7 % Output:
8 %     MImatrixcell is a series of mutual information(MI) matrix over
    the whole process
9 [nums nums_vars]=size(data);
10 [Data, av, st]=zscore(data);
11 for k=1:nums-MIsiZe+1
12     dydata=Data(k:k+MIsiZe-1,:);
13 % MImatrix is the MI matrix at time instant k
14     for i=1:nums_vars
15         for j=i:nums_vars
16             MImatrix(i,j) = mutual_information_estimation(dydata(:,i)
                ),dydata(:,j),sigma,alpha);
17             MImatrix(j,i) = MImatrix(i,j);
18         end
19     end

```



```

20 MImatrixcell{1,k} = MImatrix;
21 end
22
23 end

1 function Di = MITCSA(data,MImatrixcell,MIsized)
2 % Input:
3 %     data is the sample matrix X
4 %     MIdata is the MI matrix of data
5 %     MIsized is the length w of sliding window
6 % Output:
7 %     Di is the similarity index
8 for i=1:length(MImatrixcell)
9     MImatrix=MImatrixcell{1,i};
10 % Eigen-decomposition of the mutual information(MI) matrix
11 [Vet C]=eig(MImatrix,'vector');
12 % The MI based transform components(TCs)
13 T=data{1,i}*Vet;
14 % The statistic of TCs
15 Mu(i,:) = mean(T); % mean
16 V(i,:) = sum((T-Mu(i,:)).^2)/MIsized; % variance
17 S1(i,:) = sum((T-Mu(i,:)).^3)/MIsized;
18 K1(i,:) = sum((T-Mu(i,:)).^4)/MIsized;
19 S(i,:) = S1(i,:)/(V(i,:).^(3/2)); % skewness
20 K(i,:) = K1(i,:)/(V(i,:).^2)-3; % kurtosis
21 end
22 Oo = [Mu,V,S,K];
23 Mu_mu = mean(Mu); % the reference mean
24 Oo_mu = mean(Oo);
25 Oo_sv = std(Oo,1);
26 % The calculation of the similarity index
27 for i=1:length(MImatrixcell)
28     D1 = Oo(i,:)-Oo_mu;
29     D = D1./(Oo_sv);
30     Di(1,i) = norm(D,inf);
31 end
32
33 end

```

References

References

- [1] S. Yin, S. X. Ding, X. Xie, et al, A review on basic data-driven approaches for industrial process monitoring, IEEE Transactions on Industrial Electronics 61 (11) (2014) 6418–6428.
- [2] S. Yin, H. Gao, O. Kaynak, Data-driven control and process monitoring for industrial applications, part i, IEEE Transactions on Industrial Electronics 61 (11) (2014) 6356–6359.
- [3] J. F. Macgregor, T. Kourti, Statistical process control of multivariate processes, Control Engineering Practice 3 (4) (1995) 403–414.

- [4] R. L. Mason, J. C. Young, Multivariate statistical process control with industrial applications, *Technometrics* 46 (4) (2002) 484–485.
- [5] Y. Wang, Y. Si, B. Huang, et al, Survey on the theoretical research and engineering applications of multivariate statistics process monitoring algorithms: 2008-2017, *The Canadian Journal of Chemical Engineering* 96 (10) (2018) 2073–2085.
- [6] B. M. Wise, L. Ricker, D. F. Velthuis, B. R. Kowalski, A theoretical basis for the use of principal component models for monitoring multivariate process, *Process Control and Quality* 1 (1) (1990) 41–51.
- [7] J. V. Kresta, J. F. Macgregor, T. E. Marlin, Multivariate statistical monitoring of process operating performance, *The Canadian Journal of Chemical Engineering* 69 (1) (1991) 35–47.
- [8] J. M. Lee, C. K. Yoo, I. B. Lee, Statistical process monitoring with independent component analysis, *Journal of Process Control* 14 (5) (2004) 467–485.
- [9] S. J. Qin, Statistical process monitoring: basics and beyond, *Journal of Chemometrics* 17 (2003) 480–502.
- [10] H. Hotelling, Relations between two sets of variates, *Biometrika* 28 (3/4) (1936) 321–377.
- [11] W. Ku, R. H. Storer, C. Georgakis, Disturbance detection and isolation by dynamic principal component analysis, *Chemometrics and Intelligent Laboratory Systems* 30 (1) (1995) 179–196.
- [12] Y. N. Dong, S. J. Qin, A novel dynamic pca algorithm for dynamic data modeling and process monitoring, *Journal of Process Control* 67 (2018) 1–11.
- [13] C. Tong, T. Lan, X. Shi, Double-layer ensemble monitoring of non-gaussian processes using modified independent component analysis, *ISA transactions* 68 (2017) 181–188.
- [14] Y. W. Zhang, Y. Zhang, Fault detection of non-gaussian processes based on modified independent component analysis, *Chemical Engineering Science* 65 (16) (2010) 4630–4639.
- [15] C. D. Tong, T. Lan, X. H. Shi, Ensemble modified independent component analysis for enhanced non-gaussian process monitoring, *Control Engineering Practice* 58 (2017) 34–41.
- [16] C. Alcala, S. J. Qin, Reconstruction-based contribution for process monitoring, *Automatica* 45 (7) (2009) 1593–1600.
- [17] L. Zhang, J. Lin, R. Karim, Sliding window-based fault detection from high-dimensional data streams, *IEEE Transactions on Systems, Man, and Cybernetics: Systems* 47 (2) (2016) 289–303.

- [18] Z. W. Chen, S. Ding, T. Peng, C. H. Yang, Fault detection for non-gaussian processes using generalized canonical correlation analysis and randomized algorithms, *IEEE Transactions on Industrial Electronics* 65 (2) (2017) 1559–1567.
- [19] Q. Jiang, S. Ding, Y. Wang, X. F. Yan, Data-driven distributed local fault detection for large-scale processes based on the ga-regularized canonical correlation analysis, *IEEE Transactions on Industrial Electronics* 64 (10) (2017) 8148–8157.
- [20] J. Wang, Q. P. He, Multivariate statistical process monitoring based on statistics pattern analysis, *Industrial & Engineering Chemistry Research* 49 (17) (2010) 7858–7869.
- [21] S. M. Zhang, C. H. Zhao, Hybrid independent component analysis (h-ica) with simultaneous analysis of high-order and second-order statistics for industrial process monitoring, *Chemometrics and Intelligent Laboratory Systems* 185 (2019) 47–58.
- [22] M. S. Choudhury, S. L. Shah, N. F. Thornhill, Diagnosis of poor control-loop performance using higher-order statistics, *Automatica* 40 (10) (2004) 1719–1728.
- [23] Q. P. He, J. Wang, Statistics pattern analysis: A new process monitoring framework and its application to semiconductor batch processes, *AIChE Journal* 57 (1) (2011) 107–121.
- [24] J. Shang, M. Chen, H. Ji, et al, Recursive transformed component statistical analysis for incipient fault detection, *Automatica* 80 (2017) 313–327.
- [25] J. Shang, M. Chen, Recursive dynamic transformed component statistical analysis for fault detection in dynamic processes, *IEEE Transactions on Industrial Electronics* 65 (1) (2018) 578–588.
- [26] B. Q. Zhou, X. S. Gu, Multi-block statistics local kernel principal component analysis algorithm and its application in nonlinear process fault detection, *Neurocomputing* 376 (2020) 222–231.
- [27] G. Jia, Y. Wang, B. Huang, Dynamic higher-order cumulants analysis for state monitoring based on a novel lag selection, *Information Science* 331 (2016) 45–66.
- [28] F. Lv, C. Wen, M. Liu, Representation learning based adaptive multimode process monitoring, *Chemometrics and Intelligent Laboratory Systems* 181 (2018) 95–104.
- [29] C. H. Chang, Deep and shallow architecture of multilayer neural networks, *IEEE Transactions on Neural Networks and Learning Systems* 26 (10) (2015) 2477–2486.
- [30] G. H. Bazan, P. R. Scalassara, W. Endo, et al, Stator fault analysis of three-phase induction motors using information measures and artificial neural networks, *Electric Power Systems Research* 143 (2017) 347–356.

- [31] S. Verron, T. Tiplica, A. Kobi, Fault detection and identification with a new feature selection based on mutual information, *Journal of Process Control* 18 (5) (2008) 479–490.
- [32] M. Jiang, M. A. Munawar, T. Reidemeister, et al, Efficient fault detection and diagnosis in complex software systems with information-theoretic monitoring, *IEEE Transactions on Dependable and Secure Computing* 8 (4) (2011) 510–522.
- [33] M. M. Rashid, J. Yu, A new dissimilarity method integrating multidimensional mutual information and independent component analysis for non-gaussian dynamic process monitoring, *Chemometrics and Intelligent Laboratory Systems* 115 (2012) 44–58.
- [34] J. Yu, J. Chen, M. M. Rashid, Multiway independent component analysis mixture model and mutual information based fault detection and diagnosis approach of multiphase batch processes, *AIChE Journal* 59 (8) (2013) 2761–2779.
- [35] B. Jiang, W. Sun, R. D. Braatz, An information-theoretic framework for fault detection evaluation and design of optimal dimensionality reduction methods, *IFAC* 51 (24) (2018) 1311–1316.
- [36] A. Joshi, P. Deignan, P. Meckl, et al, Information theoretic fault detection, *Proceedings of the 2005, American Control Conference* (2005) 1642–1647.
- [37] T. M. Cover, J. A. Thomas, *Elements of information theory*, John Wiley & Sons, New York, 1991.
- [38] P. E. Latham, Y. Roudi, Mutual information, *Scholarpedia* 4 (1) (2009) 1658.
- [39] C. E. Shannon, A mathematical theory of communication, *Bell system technical journal* 27 (3) (1948) 379–423.
- [40] S. K. Jakobsen, Mutual information matrices are not always positive semidefinite, *IEEE Transactions on Information Theory* 60 (5) (2014) 2694–2696.
- [41] J. C. Principe, *Information theoretic learning: Rényi’s entropy and kernel perspectives*, Springer Science & Business Media, 2010.
- [42] T. Cover, J. Thomas, J. Wiley, *Elements of Information Theory*, Tsinghua University Press, 2003.
- [43] M. Muller-Lennert, F. Dupuis, O. Szehr, S. Fehr, M. Tomamichel, On quantum rényi’s entropies: A new generalization and some properties, *Journal of Mathematical Physics* 54 (12).
- [44] P. Bromiley, N. Thacker, E. Bouhova-Thacker, Shannon entropy, rényi’s entropy, and information, *Statistics and Inf. Series* (2004-004).
- [45] S. Yu, L. G. S. Giraldo, R. Jenssen, J. C. Principe, Multivariate extension of matrix-based rényi’s α -order entropy functional, *IEEE Transactions on Pattern Analysis and Machine Intelligence*.

- [46] B. C. Ross, Mutual information between discrete and continuous data sets, *PloS one* 9 (2) (2014) e87357.
- [47] W. Gao, S. Kannan, S. Oh, P. Viswanath, Estimating mutual information for discrete-continuous mixtures, in: *Advances in neural information processing systems*, 2017, pp. 5986–5997.
- [48] L. G. S. Giraldo, M. Rao, J. C. Principe, Measures of entropy from data using infinitely divisible kernels, *IEEE Transactions on Information Theory* 61 (1) (2015) 535–548.
- [49] R. Bhatia, Infinitely divisible matrices, *American Mathematical Monthly* 113 (3) (2006) 221–235.
- [50] J. M. Lee, S. J. Qin, I. B. Lee, Fault detection and diagnosis based on modified independent component analysis, *AIChE Journal* 52 (10) (2006) 3501–3514.
- [51] F. J. Dyson, Statistical theory of the energy levels of complex systems i, *Journal of Mathematical Physics* 3 (1) (1962) 140–156.
- [52] S. X. Ding, *Model-Based Fault Diagnosis Techniques: Design Schemes, Algorithms and Tools* (2nd ed.), Springer-Verlag, 2013.
- [53] Z. W. Chen, K. Zhang, Y. A. Shardt, S. X. Ding, et al, Comparison of two basic statistics for fault detection and process monitoring, *IFAC-Papers On Line* 50 (1) (2017) 14776–14781.
- [54] S. Yu, J. C. Principe, Simple stopping criteria for information theoretic feature selection, *Entropy* 21 (1) (2019) 99.
- [55] B. W. Silverman, *Density estimation for statistics and data analysis*, CRC press.
- [56] J. Shi, J. Malik, Normalized cuts and image segmentation, *IEEE Transactions on pattern analysis and machine intelligence* 22 (8) (2000) 888–905.
- [57] J. Downs, F. Vogel, A plant-wide industrial process control problem, *Computers and chemical engineering* 17 (3) (1993) 245–255.
- [58] N. L. Ricker, Optimal steady-state operation of the tennessee eastman challenge process, *Computers and chemical engineering* 19 (9) (1995) 949–959.
- [59] L. H. Chiang, R. D. Braatz, E. L. Russell, *Fault detection and diagnosis in industrial systems*, Springer, 2001.
- [60] E. L. Russell, L. H. Chiang, R. D. Braatz, *Data-driven methods for fault detection and diagnosis in chemical processes*, Springer, 2012.
- [61] Z. Chen, H. Fang, Y. Chang, Weighted data-driven fault detection and isolation: a subspace-based approach and algorithms, *IEEE Transactions on Industrial Electronics* 63 (5) (2016) 3290–3298.

- [62] G. Apali, C. F. Alcala, S. J. Qin, D. Zhou, Generalized reconstruction-based contributions for output-relevant fault diagnosis with application to the tennessee eastman process, *IEEE Transactions on Control Systems Technology* 19 (5) (2011) 1114–1127.